JOURNAL OF THE ROYAL SOCIETY Interface

J. R. Soc. Interface (2006) **3**, 689–697
doi:10.1098/rsif.2006.0135
Published online 30 May 2006

Wet but not slippery: boundary friction in tree frog adhesive toe pads

W. Federle[1,2,*], W. J. P. Barnes[3], W. Baumgartner[4], P. Drechsler[1,2] and J. M. Smith[3]

[1]*Department of Zoology, University of Cambridge, Cambridge CB2 3EJ, UK*
[2]*Zoology II, University of Würzburg, Biozentrum, 97074 Würzburg, Germany*
[3]*Division of Environmental and Evolutionary Biology, Institute of Biomedical and Life Sciences, University of Glasgow, Glasgow G12 8QQ, UK*
[4]*Department of Cellular Neurobionics, Institute of Biology 2, RWTH-Aachen, 52056 Aachen, Germany*

Tree frogs are remarkable for their capacity to cling to smooth surfaces using large toe pads. The adhesive skin of tree frog toe pads is characterized by peg-studded hexagonal cells separated by deep channels into which mucus glands open. The pads are completely wetted with watery mucus, which led previous authors to suggest that attachment is solely due to capillary and viscous forces generated by the fluid-filled joint between the pad and the substrate. Here, we present evidence from single-toe force measurements, laser tweezer microrheometry of pad mucus and interference reflection microscopy of the contact zone in *Litoria caerulea*, that tree frog attachment forces are significantly enhanced by close contacts and boundary friction between the pad epidermis and the substrate, facilitated by the highly regular pad microstructure.

Keywords: biomechanics; adhesion; Hylidae; interference reflection microscopy; microrheology

1. INTRODUCTION

The dynamic mechanisms of adhesion used by different animals have become an important research area in recent years because of the increased feasibility of fabricating biomimetic adhesives (Autumn *et al.* 2002; Geim *et al.* 2003; Sitti & Fearing 2003). Adhesive systems in many animals are 'wet', i.e. supplemented by a fluid secreted into the contact zone (Scherge & Gorb 2001). A continuous fluid film in the contact zone is expected to act as a lubricant so that pads should easily slide. However, the capacity to sustain adequate friction appears fundamental to animal locomotion and maneuverability (Radhakrishnan 1998). How can animals generate sufficient friction despite a fluid-based adhesion mechanism?

We investigate this question in the adhesive system of tree frogs. Several families, including Hylidae, Rhacophoridae, Microhylidae and Dendrobatidae have independently evolved adhesive toe pads, i.e. disc-like, flattened enlargements of the tips of the digits, which all show a similar, specialized epidermal architecture and structure. Toe pads provide a firm grip on smooth leaf and branch surfaces. Analogous in morphology and function to adhesive pads in some insects (Gorb *et al.* 2000; Beutel & Gorb 2001), tree frog toe pads are soft and patterned with a regular hexagonal microstructure of approximately 10 µm diameter epidermal cells separated by approximately 1 µm wide channels; the flattened surface of each cell features a similar but much finer microstructure of approximately 0.1–0.4 µm diameter pegs which originate from hemidesmosomes (Ernst 1973*a*; Welsch *et al.* 1974; Mizuhira 2004; figure 1). The cellular and subcellular surface architecture differs significantly from that of all other epidermal cells of these frogs (Ernst 1973*a*; Green 1979). Subdivision of the contact zone into microscopic subunits has been recognized as a general design principle in animal adhesive pads (Autumn *et al.* 2002; Arzt *et al.* 2003). Microstructured adhesives can show greater adhesion (Peressadko & Gorb 2004; Chung & Chaudhury 2005), which may be due either to their better capacity to conform to rough surfaces, to crack arresting (Hui *et al.* 2004; Chung & Chaudhury 2005), or to length-specific scaling of the subcontacts' pull-off forces (Arzt *et al.* 2003). These benefits, however, may be less important in tree frogs and many insects, where a fluid film is present in the adhesive contact zone.

Tree frog adhesive pads are permanently wetted by mucus secreted from glands that open into the channels between epidermal cells (Ernst 1973*b*). Earlier authors assumed a glue-like function of the mucus (Dewitz 1884), but this was not confirmed by later experimental studies (Emerson & Diehl 1980; Hanna & Barnes 1991). Instead, a consensus has been reached that tree frogs

*Author for correspondence (wf222@cam.ac.uk).

Received 10 April 2006
Accepted 9 May 2006

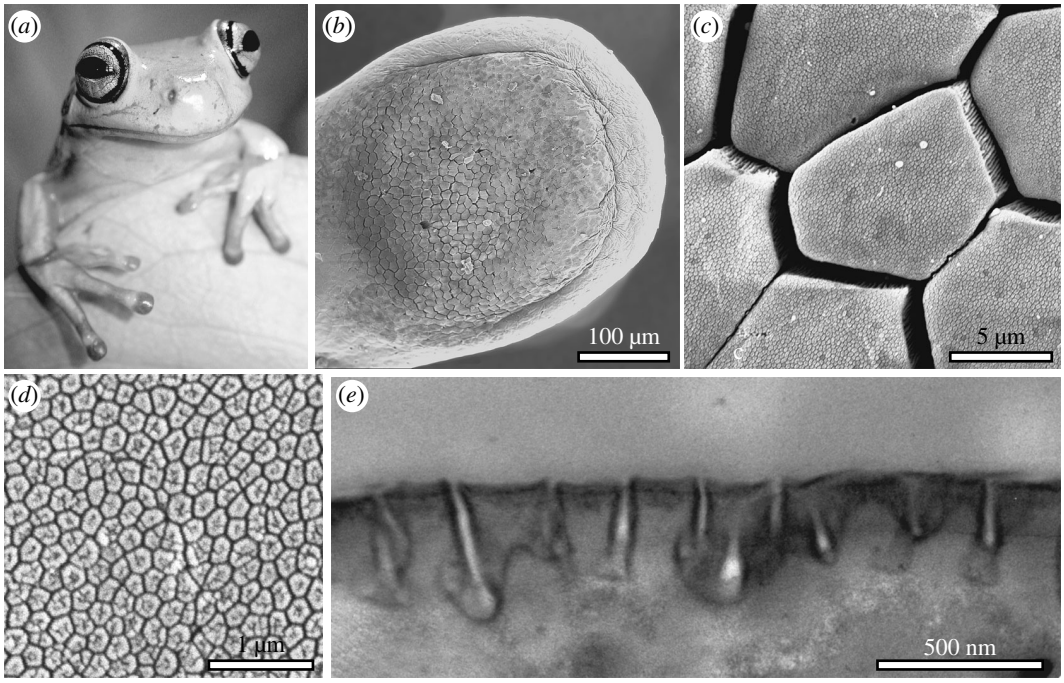

Figure 1. Morphology of tree frog toe pads. (*a*) White's tree frog (*Litoria caerulea*). (*b–d*) SEMs of (*b*) toe pad, (*c*) epidermis with hexagonal epithelial cells and (*d*) high power view of the surface of a single hexagonal cell showing peg-like projections. (*e*) TEM of cross-section through cell surface.

stick to surfaces by using 'wet adhesion', i.e. the combined forces of surface tension and viscosity generated by a continuous, fluid-filled joint between the pad and the substrate (Nachtigall 1974; Emerson & Diehl 1980; Green 1981; Hanna & Barnes 1991; Barnes 1999; Barnes *et al.* 2002). Several lines of evidence have been provided to support this hypothesis. First, there is a visible meniscus around the area of contact between the pad and the substrate; second, shear forces of toe pads were found to be velocity-dependent (Hanna & Barnes 1991); and third, the sticking ability of frogs was reduced when toe pads were immersed in water (Emerson & Diehl 1980). Recent work on *Colostethus trinitatis* (Barnes *et al.* 2002), however, showed that these freshwater frogs are capable of climbing on wet rock using their toe pads, even when water is flowing over the substrate.

Hence, we test in this study whether the model of a continuous fluid film provides an adequate description of the attachment mechanism of White's tree frogs (*Litoria caerulea*, Hylidae). We aim to achieve this by measuring firstly the thickness of the fluid layer between the pad and the substrate, secondly the viscosity of the toe pad mucus, and thirdly the static and dynamic shear stress generated by single toe pads.

2. MATERIAL AND METHODS

2.1. In vivo *interference reflection microscopy of the toe pad contact zone*

Frogs were placed in an inverted position in polystyrene Petri dishes (diameter 86 mm; height 17 mm) with two large rectangular holes cut into the bottom covered by 24×60 mm glass cover-slips so that toe pads in contact with glass could be observed. We used a Leica DMR-HC upright microscope equipped with switchable bandpass interference filters in the epi-illumination path to isolate the 546 or 436 nm lines from the spectrum of a 100 W mercury arc lamp. The illuminating numerical aperture (INA) could be set to 0.27, 0.79 or 1.27 using a home-built pinhole slider. Images were captured using a 12 bit monochrome digital camera (QIC-FM12, QImaging). After calibration of the optical system, relative intensities were calculated from image grey-scale values (Baldock & Poole 1993).

Illumination and exposure time were adjusted to obtain the interference maxima and minima over the full grey-scale range in which the camera response was linear (approx. 100–3000). To determine the order of the interference fringes, toe pads were imaged using varying wavelengths and INAs. The refractive index of toe pad mucus was measured with a refractometer (ATAGO, L. Kübler, Karlsruhe, Germany) by collecting 2 µl samples of the fluid with fine capillaries ($n=5$); it was found to be only slightly higher than that of water ($n=1.335$). The fluid film thickness in the centre of the hexagons was determined by comparing the measured interference patterns with theoretical predictions (see appendix B, Gingell & Todd 1979; Rädler & Sackmann 1993; Aveyard *et al.* 1996). We analysed 84 hexagons from 20 toes and five frogs.

2.2. *Microrheometry of toe pad mucus*

To measure the rheology of toe pad mucus, a laser tweezer technique was used. We prepared glass cover-slips covered with a thin layer of 2.8 µm diameter fluorescent latex beads (Dynabeads M-280, Dynal, Hamburg, Germany). Beads were washed twice in distilled H_2O and droplets of the solution were evaporated on the cover-slip surface. To obtain samples

of toe pad mucus, we carefully dabbed single toes of *L. caerulea* frogs onto the bead-covered cover-slip, which formed the wall of a small circular container (2 cm diameter). To minimize evaporation, footprints were collected and sealed inside the vial within less than 10 s. The cover-slip was placed on a piezo-controlled XY stage on an Axiovert 135 microscope (Zeiss, Oberkochen, Germany) equipped with a home-built laser tweezer. The set-up consisted of a Nd : YAG laser (1064 nm), the beam of which was expanded to fill the back aperture of a high NA-objective (100×1.3 oil, Plan Neofluar, Zeiss), coupled through the epi-illumination port of the microscope and reflected to the objective by a dichroic mirror (FT510, Zeiss). The laser intensity was adjusted to 50 mW in the focal plane. Fluid viscosity was measured by moving the stage with the fluid droplet sinusoidally perpendicular to the optical axis (amplitude: approximately 10 µm, frequency: 0.5–5 Hz), while a single bead was held in the focus of the laser beam. The passing fluid exerts a drag force on the bead (which is linearly dependent on velocity; $Re \approx 2\times10^{-6}$), causing a small lateral displacement of the bead. Bead and substrate position were extracted from video recordings with an accuracy of approximately 50 nm using an automatic image analysis routine (Schmidt *et al.* 1995). Displacement was fitted with a sine function to determine the phase and amplitude of the elicited movement. By comparing bead displacement in frog mucus and in droplets of distilled water (measured under identical conditions), mucus viscosity was calculated from the slopes of the regression of bead displacement amplitude against oscillation frequency (figure 3*c*).

2.3. Measurement of shear stress in frog toe pads

Litoria caerulea frogs were placed in polystyrene Petri dishes (diameter 86 mm, height 17 mm) with 30 holes of 7–10 mm diameter drilled into the bottom. A frog held in the inverted position could easily be made to expose a single toe through one of the holes. By moving the Petri dish attached to a micromanipulator, the toe was brought into contact with a 10×12.5 mm glass cover-slip mounted on a home-built two-dimensional strain gauge force transducer. The transducer consisted of a phosphor bronze bending beam machined with a 90° twist with two half-bridges of bonded foil strain gauges (BLH Electronics, Heidelberg) to measure normal and shear force directions. Friction experiments were conducted by moving the force transducer using a computer-controlled motorized XYZ micromanipulator (M-126, Physik Instrumente). Pad preload was adjusted manually to be approximately 1 mN. A closed feedback loop kept the normal load constant at 0.1 mN during the friction experiment. The glass surface was moved by 10 mm at a constant velocity of 500 µm s^{-1}. Shear forces were recorded (i) at the onset of pad sliding; (ii) during steady sliding (at the end of the movement); and (iii) 2 min after the movement had stopped (see figure 4*a*). To assess the possibility of very slow, residual sliding after the end of the motor movement, we measured the pad position during the 2 min after the motor had stopped and performed a second order polynomial fit. The glass surface was carefully cleaned with distilled water and acetone using lens paper after each trial to remove any mucus residues. We used an ultrasonic humidifier (Honeywell, BH-860 E) to perform the measurements at greater than 80% air humidity (20 °C). To calculate shear stress (the ratio of shear force and contact area) we measured the contact area of the toe pads during the force measurements, using reflected light video images (Federle & Endlein 2004).

3. RESULTS AND DISCUSSION

In vivo interference reflection microscopy (IRM) of *L. caerulea* toe pads adhering to glass revealed that the centres of the hexagonal cells (and specifically, the peg-like hemidesmosomes on their surface) come into closest contact with the substrate (figure 2*a–c*). Images taken with green ($\lambda = 546$ nm) and blue ($\lambda = 436$ nm) light and different INAs (INA = 0.27 and 1.27) show that most of the hexagonal cells had dark zones in the centre, which correspond to zero order interference minima (i.e. to a mucus film thickness less than 100 nm). We base this on the observation that firstly, the centres of the hexagonal cells were dark for both illuminating wavelengths (figure 2*a*,*b*), secondly the position of second order 'green' minima coincided with second order 'blue' maxima as predicted from theory (figure 2*d*; since $\lambda_{blue}/\lambda_{green} \approx 4/5$), and thirdly that they remained visible even for the largest INA (figure 2*c*), where we would expect all but the zero order interference fringes to be strongly dampened (appendix B; Gingell & Todd 1979; Rädler & Sackmann 1993). The uniform reflectivity of most epidermal cells indicated that they had a similar, small distance to the substrate. Epidermal cells further away from the substrate had a convex contour, whereas cells in close contact were typically deformed and flattened (as indicated by the large size of the central dark areas (figure 2*a–c*,*e*). We quantified the thickness of the mucus layer by measuring the brightness of the central areas of cells in close contact and comparing it to the zero order maximum and the first order minimum (INA = 0.27, see appendix B). Film thickness ranged from 0 to 35 nm and was indistinguishable from zero in many hexagons (median 6.0 nm, figure 2*f*). Thus, the IRM analysis shows that the fluid films in the centre of epidermal cells were extremely thin, and that some parts of the toe pad cells may have even made direct ('dry') contact to the glass substrate.

Using a laser tweezer technique we showed that *L. caerulea* toe pad mucus is low-viscous. 2.8 µm latex spheres immersed in a droplet of toe pad mucus were trapped in the focus of a laser beam. When we applied a sinusoidal movement of the fluid, the sphere was laterally displaced by drag forces. The elicited movement of the sphere was almost perfectly sinusoidal (no trend visible in residuals of least square sinusoidal fit) and phase-shifted by approximately 90° against the movement of the fluid (figure 3*b*). This indicates that the fluid secreted by the toe mucus glands has, in first approximation, Newtonian properties. By comparing

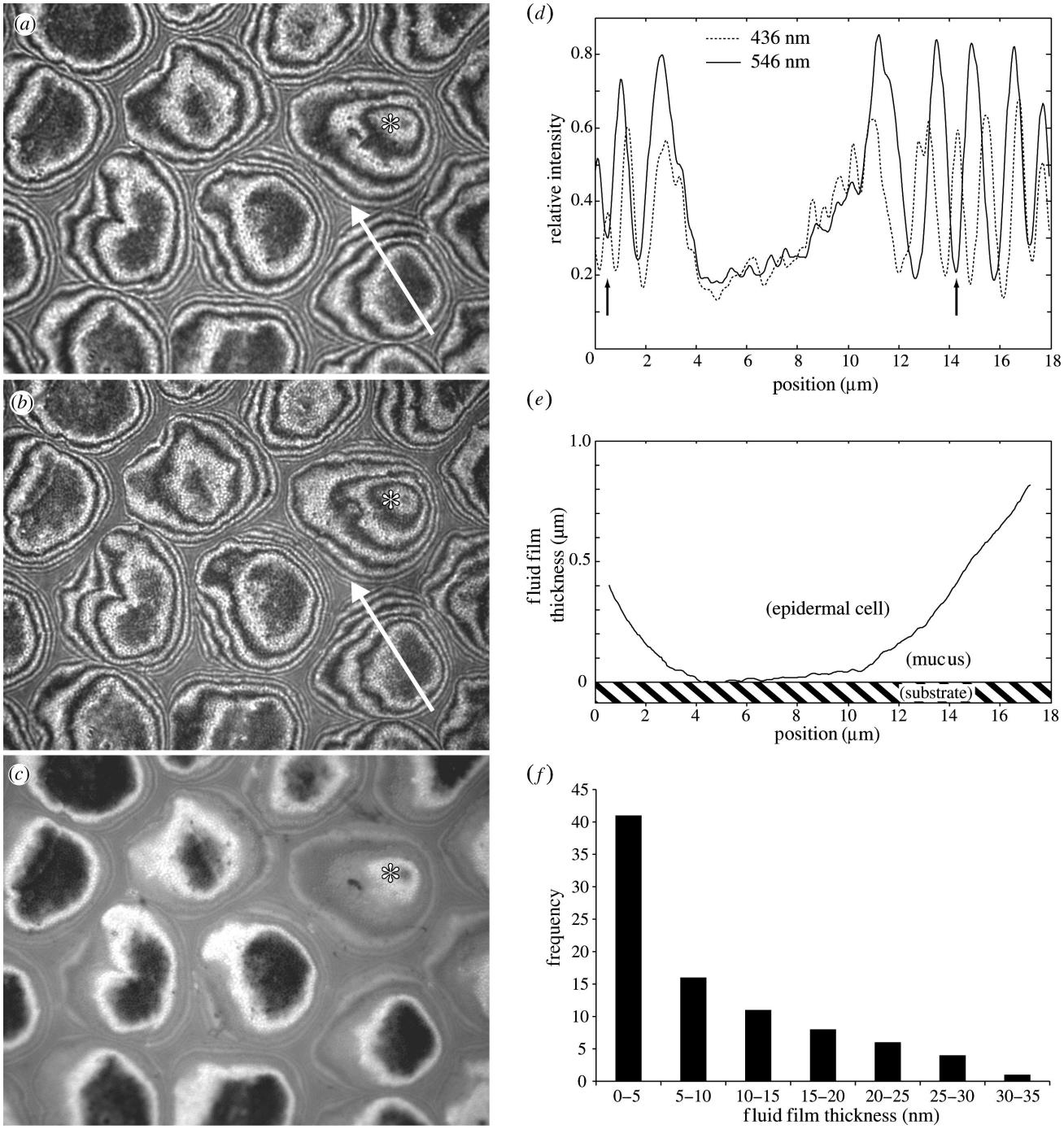

Figure 2. *In vivo* analysis of *Litoria caerulea* toe pad contact with glass using interference reflection microscopy (IRM). (*a–c*) Corresponding images of the same area of the contact zone taken using different wavelengths and illuminating numerical apertures (INA): (*a*) 546 nm, INA = 0.27, (*b*) 436 nm, INA = 0.27, and (*c*) 546 nm, INA = 1.27. Note the hemidesmosome pegs visible as dark spots in the central cell areas. Asterisks denote one epidermal cell, which is not in close contact ($h \geq 40$ nm) and has a convex shape. (*d*), Intensity profile along the arrow shown in (*a*) and (*b*). Arrows indicate the position of the second order 'green' minimum coinciding with the second order 'blue' maximum. (*e*) Reconstruction of the fluid film thickness along the arrow shown in (*a*) and (*b*) (see appendix B). (*f*) Frequency of measured fluid film thicknesses in hexagons with zero order minimum ($n = 87$ from five frogs).

bead displacement in frog mucus and in water, we measured mucus viscosity to range from 1.25 to 1.51 mPa s (mean 1.43 mPa s; $n = 8$ measurements using three different frogs, figure 3*c*).

Shear stress measurements on single *L. caerulea* toe pads demonstrated that pads generate static friction. Static friction was not only evident from the build-up of force at the onset of sliding (figure 4*a,b*, median shear stress 1.08 kPa) but also from the presence of a remaining shear force 2 min after the sliding motion had stopped (figure 4*a,b*, median shear stress 1.12 kPa). As extremely slow sliding could be misinterpreted as 'static' contact, we measured the amount of pad sliding during the 2 min after the motor had stopped and performed a second order polynomial fit of pad position. This analysis indicated that, if the pads had indeed still

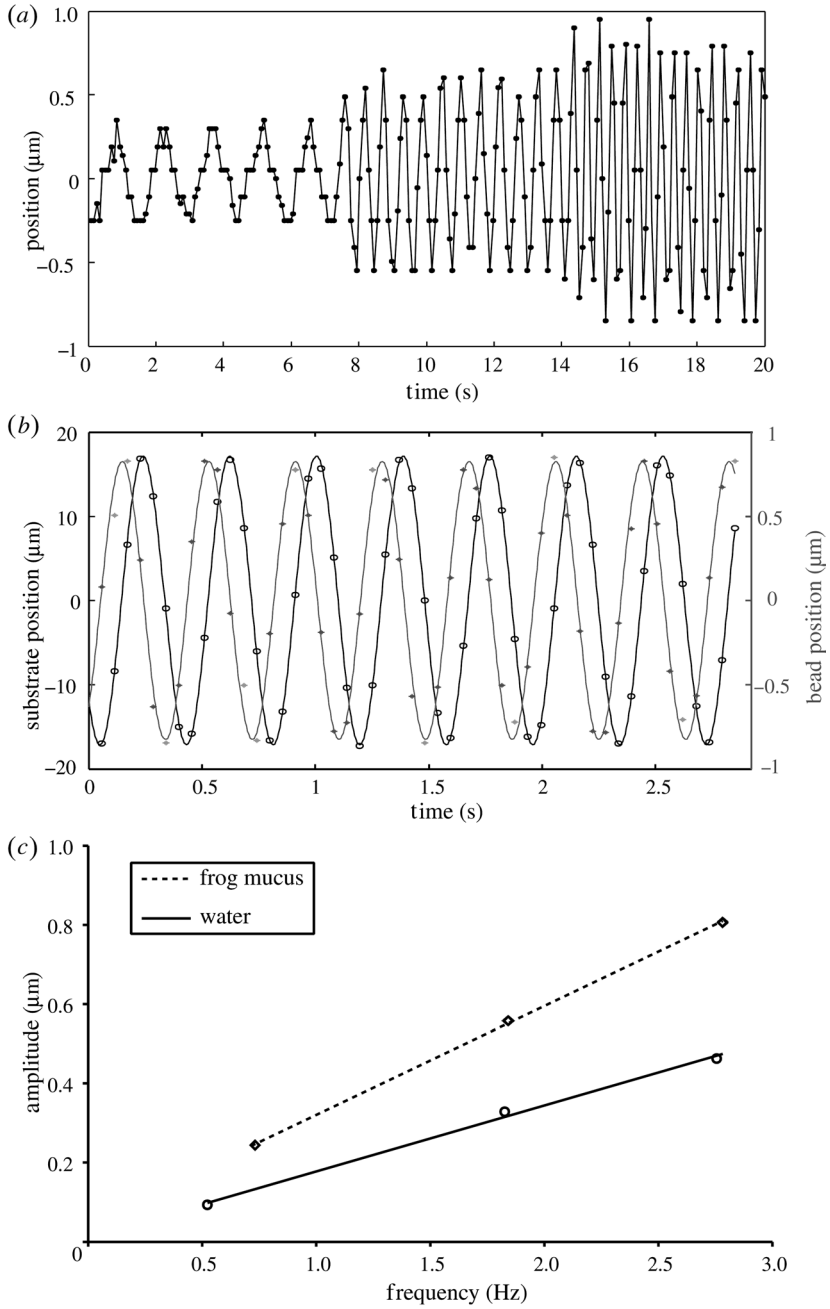

Figure 3. Microrheology of *Litoria caerulea* toe pad mucus using laser tweezers. (*a*) Bead displacement elicited by sinusoidal fluid movement at three different frequencies. (*b*) Sinusoidal fit of bead and fluid (=substrate) movement. Here, bead displacement was phase-shifted by 87.0° against the movement of the fluid. (*c*) Relationship of bead displacement amplitude and velocity (frequency) measured for toe pad mucus and pure water. The slopes indicate that this sample of toe pad mucus was 1.65 times more viscous than water.

been sliding after 2 min, the mean remaining sliding velocity was less than 33 nm s^{-1}. Assuming a continuous mucus film of thickness d to be present in the entire pad contact zone, the film thickness predicted from simple hydrodynamic lubrication ($d=\eta v/\sigma \cong 1.5\times 10^{-4}$ nm) is much less than a single molecular layer of water. An analogous calculation for pads sliding at 500 µm s^{-1} velocity yields film thicknesses in the order of 1–2 water layers ($d=\eta v/\sigma \cong 0.4$ nm). The static shear stress is also too large to be explained by the deformation and resulting retentive force of the fluid film's meniscus (appendix A). Thus, the measured shear forces are inconsistent with hydrodynamic lubrication and a continuous fluid film between the pad and the substrate. The traction of frog toe pads on a surface does, therefore, not result primarily from the viscosity and surface tension of the mucus film, but from boundary friction of the toe pad epidermis on the substrate (Persson 1998). Boundary friction may be based on the formation of dry contacts by the dewetting of an intercalated fluid film (Brochard-Wyart & de Gennes 1994; Martin *et al.* 2000). Moreover, a thin layer of mucus remaining between the pad and the substrate could behave like a solid because of possible non-Newtonian properties or molecular ordering due to confinement (Granick 1991; Zhang *et al.* 2002).

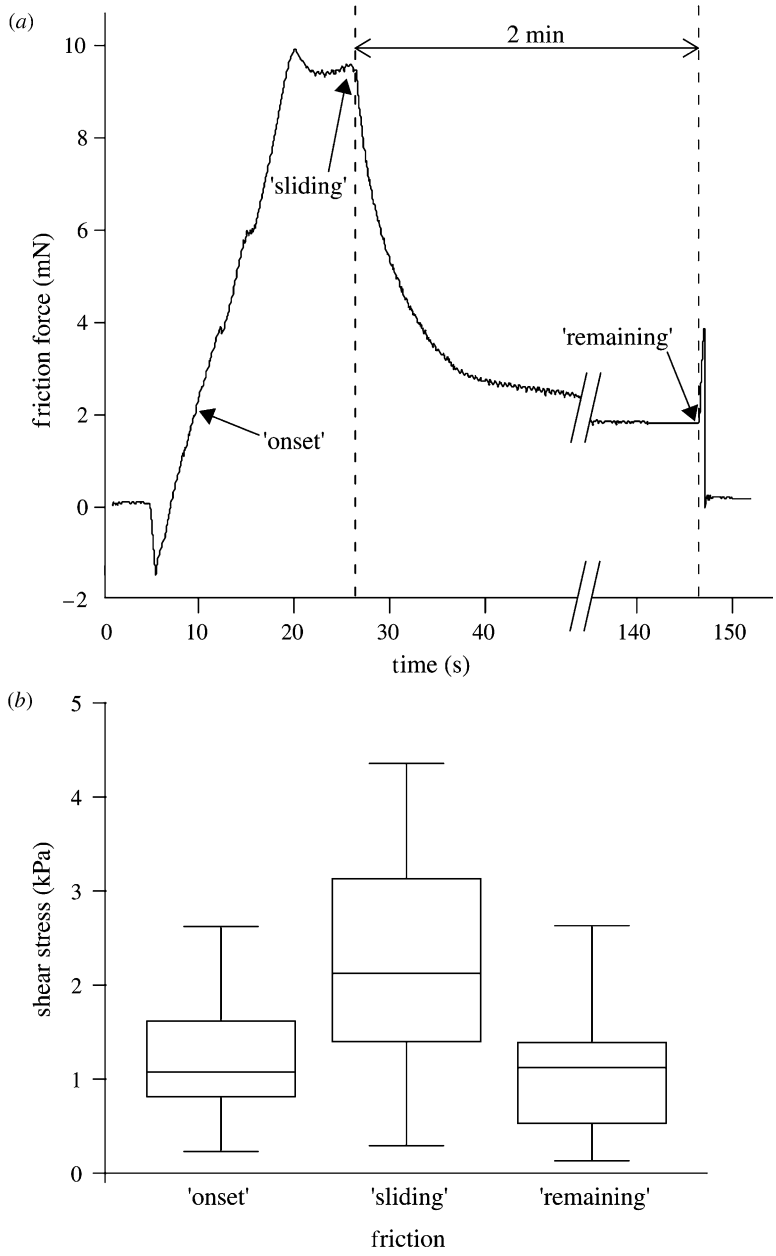

Figure 4. Shear stress measurement in single toe pads of *Litoria caerulea*. (*a*) Friction force during a sliding experiment consisting of 20 s sliding toward the body (500 µm s^{-1}) followed by 2 min standstill. (*b*) Toe pad shear stress at the transition from rest to sliding ('onset'), during steady sliding ('sliding') and 2 min after the end of the motor movement ('remaining'). Centre lines denote medians; boxes, the inner two quartiles; and whiskers, the upper and lower 5%. Data from 10 toe pads of three frogs.

Although wet adhesion is necessary to hold on at angles beyond the vertical, the capacity of animals to generate sufficient shear forces on leaf and branch surfaces represents an essential component of arboreal locomotion. Resistance against shear forces and slipping is not only required when frogs walk or rest on a vertical surface. Due to the sprawled posture, they are also involved when frogs stand upright or hang upside-down. Independent of the detailed physical mechanism, tree frogs can only generate sufficient friction by bringing their toe pads into very close contact to the surface. When toe pads are put down, fluid has to be squeezed out of the contact zone to prevent hydrodynamic lubrication. During walking, this task has to be accomplished very rapidly. The time required for two parallel disks of radius R immersed in a liquid of viscosity η to approach each other a given distance h_2-h_1 under a load F is predicted to be (Reynolds 1886):

$$t_{\mathrm{R}} = \frac{3\pi}{4}\,\frac{\eta R^4}{F_{\mathrm{R}}}\left(\frac{1}{h_1^2}-\frac{1}{h_2^2}\right). \tag{3.1}$$

Thus, approach time is dependent on the thickness of the fluid film, rapidly increasing as the film gets thinner. For example, thinning a mucus film from 20 to 10 nm (for a 1 mm^2 pad loaded with 1 mN) would take more than 50 min. Clearly, a less viscid mucus will drain more easily. Mucus drainage will also be facilitated if the pad surface is not perfectly flat, but contains channels in which the liquid can flow away. If these

grooves divide a pad surface into n separate smaller contact zones (of radii $r < R/\sqrt{n}$), the drainage time will be n times shorter, because $F_r = F_R/n$ and $t_r \propto r^4/F_r \propto t_R/n$. The two-level microstructure of tree frog toe pads consisting of epidermal cells and peg-like projections is probably essential to facilitate mucus drainage and to conform to irregular substrates. Flexibility and rapid drainage of water films is also critical for the grip of car tires on wet roads (Roberts 1971). The apparent analogy in design between the microstructure of frog toe pads and the patterned profile of car tires may be based on similar requirements. We anticipate tree frog adhesion to provide a useful model for the development of improved anti-slip and holding devices, particularly those that operate in wet conditions.

We thank M. Riehle for comments on the manuscript, S. Busch and D. Roth for assistance in the shear stress measurements and T. Endlein for figure 1*a*. Supported by the German Research Foundation (SFB 567 and Emmy-Noether Fellowship to W.F.), the UK Natural Environment Research Council and the Wellcome Trust (to W.J.P.B. and J.M.S.).

APPENDIX A. POSSIBLE CONTRIBUTION OF SURFACE TENSION FORCES TO SHEAR STRESS

It is possible that surface tension forces of the mucus film contribute to static and dynamic shear forces. When the toe pad slides across the surface, the fluid meniscus will be deformed so that the contact angle with the substrate may become larger at the leading and smaller at the trailing edge. The retentive force acting on a thread of fluid moving through a tube is (West 1911):

$$F = 2\pi r \gamma_L (\cos \alpha_2 - \cos \alpha_1), \tag{A 1}$$

where $2\pi r$ is the inner perimeter of the tube, γ_L the fluid's surface tension and α_1, α_2 are the advancing and receding contact angles, respectively. For simplicity, we model the contact area as a square (side length B) and assume the contact angle deformation to be constant over the leading and trailing edges of the pad contact zone.

The static shear force for one pad due to surface tension is:

$$F = 2B\gamma_L (\cos \alpha_2 - \cos \alpha_1) \ll 4B\gamma_L. \tag{A 2}$$

Estimating B as $2\times(\text{contact area}/\pi)^{-0.5} \approx 2.6$ mm and the surface tension of mucus (70 mN m^{-1}), we obtain:

$$F \ll 4B\gamma_L \approx 0.73 \text{ mN}. \tag{A 3}$$

With a pad contact area of 5.3 ± 1.8 mm^2 (mean $\pm$ s.d.) this maximal estimate corresponds to a static shear stress of 0.14 kPa, which is considerably less than the measured static shear stress (figure 4*b*). Thus, the presence of static shear stress in frog toe pads cannot be explained by surface tension forces alone.

APPENDIX B. INTERFERENCE REFLECTION MICROSCOPY—THEORY AND IMAGE ANALYSIS

Expected interference fringe patterns were calculated according to Gingell & Todd (1979) and Aveyard *et al.* (1996). In brief, light falling from the immersion objective lens onto the glass–mucus interface (interface 1) at angle θ_0 is partially reflected and the transmitted beam is refracted. The refracted ray is partially reflected at the mucus–epidermis interface (interface 2), and this reflected ray interferes with the ray reflected from interface 1. The Fresnel reflectance coefficients at the ith interface (s and p components for vertical and parallel polarized light) are given by

$$r_{ip} = \frac{n_i \cos\theta_{i-1} - n_{i-1}\cos\theta_i}{n_i \cos\theta_{i-1} + n_{i-1}\cos\theta_i} \quad \text{and}$$
$$r_{is} = \frac{n_i \cos\theta_i - n_{i-1}\cos\theta_{i-1}}{n_i \cos\theta_i + n_{i-1}\cos\theta_{i-1}}, \tag{B 1}$$

where n_0, n_1 and n_2 are the refractive indices of glass, mucus and epidermis, respectively, and the angles θ_i are obtained from θ_0 using Snell's law. The phase difference δ between the rays reflected from the interfaces 1 and 2 is

$$\delta = \frac{2\pi n_1 d \cos\theta_1}{\lambda}, \tag{B 2}$$

where d is the mucus film thickness and λ the wavelength. The reflectance from the two-interface system is

$$r_{1\_2} = \frac{r_1^2 + 2r_1 r_2 \cos 2\delta + r_2^2}{1 + 2r_1 r_2 \cos 2\delta + r_1^2 r_2^2}. \tag{B 3}$$

The overall reflectance is given by the mean of the r_{1_2} values obtained using the s and p components of the Fresnel coefficients. The interference pattern results from a cone of light with incidence angles θ_0 ranging from 0 to θ_{max}, as determined by the INA of the microscope. The overall interference intensity is the sum (over all incidence angles from 0 to θ_{max}) of the intensities weighted by a factor W given by (Gingell & Todd 1979)

$$W = \sin\theta_0 \cos^2\theta_0. \tag{B 4}$$

The reflected intensity normalized with respect to the reflectivity of a glass–air interface is

$$R_{(d)} = \sum_0^{\theta_{max}} (W r_{1\_2}) \Big/ \sum_0^{\theta_{max}} (W r_{air}). \tag{B 5}$$

A computer program was used to calculate $R_{(d)}$ as a function of film thickness, refractive indices, wavelength and INA. We compared the prediction for the fringe pattern (calculated using the above method) with the theory by Rädler & Sackmann (1993):

$$R_{(d)} = \Big[r_{01}^2 + (1-r_{01}^2)^2 r_{12}^2 + 2\sqrt{r_{01}^2 (1-r_{01}^2)^2 r_{12}^2} \times \frac{\sin(y)}{y} \cos(4\pi n_1 d/\lambda (1 - \sin^2\alpha/2) + \delta) \Big] / r_{0\_air}^2, \tag{B 6}$$

where $\alpha = \arcsin(\mathrm{INA}/n_1)$ and $y = 4\pi n_1 d/\lambda \sin^2\alpha/2$; a phase shift of $\delta = \pi$ occurs if one of the interfering beams is reflected at an interface to a medium with higher refractive index. Even though this approach has been developed specifically for the 'Antiflex' reflection contrast version of IRM (Ploem 1975), which employs circularly polarized light, both theories (equations (B 5) and (B 6)) predict almost identical fringe patterns (observed difference for phase less than 2% and amplitude less than 10%).

We measured the mucus film thickness between the pad and the substrate by comparing fringe patterns measured from toe pad IRM images (figure 2) with the theoretical prediction. As the amplitude of interference fringes decays like $\sin(y)/y$ (equation (B 6)), the interference pattern is almost perfectly sinusoidal for small INAs. We used the smallest aperture of our microscope (INA = 0.27), where fringe dampening in films thinner than 500 nm is negligible (less than 0.1%). Film thickness d was calculated from the intensity of the hexagon centres (I_H, measured as the mean intensity along a stretch of greater than 1.5 μm), of the zero order maximum (I_1) and of the first order minimum (I_2):

$$d = \frac{\arccos[(I_1 + I_2 - 2I_\mathrm{H})/(I_1 - I_2)]\lambda}{4\pi n_1(1 - \sin^2\alpha/2)}. \qquad \text{(B 7)}$$

The position of the zero-order maximum and the first order minimum was used to determine the local slope of the hexagon surface. As the finite aperture interference theory (Gingell & Todd 1979; Rädler & Sackmann 1993) becomes inaccurate for interfaces that exhibit larger inclinations (Wiegand *et al.* 1998), we only included measurements from hexagons with slopes smaller than 10°.

The brightness of epidermal cells measured in our analysis actually represents the pooled reflectivity of the hexagonally arranged hemidesmosome pegs (which are visible as dark spots) and of the mucus-filled channels in between them. TEM and SEM of *L. caerulea* toe pads (figure 1) shows that the hemidesmosome pegs have a maximum width of approximately 310 nm and the channels in between them are approximately 220 nm deep and approximately 25 nm wide. Reflection from the bottom of these channels could conceivably cause a second interference pattern phase-shifted to the reflection from the hemidesmosome pegs by:

$$\delta = 4\pi n_1(1 - \sin^2\alpha/2)220\ \mathrm{nm}/\lambda. \qquad \text{(B 8)}$$

Incoherent summation of the two interference patterns (weighted by the relative area of pegs (approx. 80%) and channels (approx. 20%)) would then result in a small (approx. 2 nm) shift of the zero order minimum. However, because of the narrowness of the gaps in between the pegs, most light reaching the bottom of these channels will not re-enter the microscope after reflection (this is also evident from the background of the pegs, which appears uniformly grey and does not show any interference effects, see figure 2*a–c*). Thus, interference patterns on frog toe pads represent the reflections from the surface of the hemidesmosomes.

REFERENCES

Arzt, E., Gorb, S. & Spolenak, R. 2003 From micro to nano contacts in biological attachment devices. *Proc. Natl Acad. Sci.* **100**, 10 603–10 606. (doi:10.1073/pnas.1534701100)

Autumn, K. *et al.* 2002 Evidence for van der Waals adhesion in gecko setae. *Proc. Natl Acad. Sci.* **99**, 12 252–12 256. (doi:10.1073/pnas.192252799)

Aveyard, R., Binks, B. P., Cho, W. G., Fisher, L. R., Fletcher, P. D. I. & Klinkhammer, F. 1996 Investigation of the force-distance relationship for a small liquid drop approaching a liquid–liquid interface. *Langmuir* **12**, 6561–6569. (doi:10.1021/la9607868)

Baldock, R. A. & Poole, I. 1993 Video camera calibration for optical densitometry. *J. Microsc.* **172**, 49–54.

Barnes, W. J. P. 1999 Tree frogs and tire technology. *Tire Technol. Int.* **99**, 42–47.

Barnes, W. J. P., Smith, J., Oines, C. & Mundl, R. 2002 Bionics and wet grip. *Tire Technol. Int.* **2002**, 56–60.

Beutel, R. G. & Gorb, S. N. 2001 Ultrastructure of attachment specializations of hexapods (Arthropoda): evolutionary patterns inferred from a revised ordinal phylogeny. *J. Zool. Syst. Evol. Res.* **39**, 177–207. (doi:10.1046/j.1439-0469.2001.00155.x)

Brochard-Wyart, F. & de Gennes, P. G. 1994 Dewetting of a water film between a solid and a rubber. *J. Phys.: Condens. Matter* **6**, A9–A12. (doi:10.1088/0953-8984/6/23A/002)

Chung, J. Y. & Chaudhury, M. K. 2005 Roles of discontinuities in bio-inspired adhesive pads. *J. R. Soc. Interface* **2**, 55–61. (doi:10.1098/rsif.2004.0020)

Dewitz, H. 1884 Über die Fortbewegung der Thiere an senkrechten Flächen vermittels eines Secretes. *Pflügers Arch. Ges. Physiol.* **33**, 440–481. (doi:10.1007/BF01628473)

Emerson, S. B. & Diehl, D. 1980 Toe pad morphology and mechanisms of sticking in frogs. *Biol. J. Linn. Soc.* **13**, 199–216.

Ernst, V. V. 1973*a* The digital pads of the tree frog *Hyla cinerea*. I. The epidermis. *Tissue Cell* **5**, 83–96.

Ernst, V. V. 1973*b* The digital pads of the tree frog *Hyla cinerea*. II. The mucous glands. *Tissue Cell* **5**, 97–104.

Federle, W. & Endlein, T. 2004 Locomotion and adhesion: dynamic control of adhesive surface contact in ants. *Arthropod Struct. Dev.* **33**, 67–75. (doi:10.1016/j.asd.2003.11.001)

Geim, A. K., Dubonos, S. V., Grigorieva, I. V., Novoselov, K. S., Zhukov, A. A. & Shapoval, S. Y. 2003 Microfabricated adhesive mimicking gecko foot-hair. *Nat. Mater.* **2**, 461–463. (doi:10.1038/nmat917)

Gingell, D. & Todd, I. 1979 Interference reflection microscopy: a quantitative theory for image interpretation and its application to cell-substratum separation measurement. *Biophys. J.* **26**, 507–526.

Gorb, S., Jiao, Y. & Scherge, M. 2000 Ultrastructural architecture and mechanical properties of attachment pads in *Tettigonia viridissima* (Orthoptera Tettigoniidae). *J. Comp. Physiol. A* **186**, 821–831. (doi:10.1007/s003590000135)

Granick, S. 1991 Motions and relaxatons of confined liquids. *Science* **253**, 1374–1379.

Green, D. M. 1979 Tree frog toe pads: comparative surface morphology using scanning electron microscopy. *Can. J. Zool.* **57**, 2033–2046.

Green, D. M. 1981 Adhesion and the toe pads of tree frogs. *Copeia* **1981**, 790–796. (doi:10.2307/1444179)

Hanna, G. & Barnes, W. J. P. 1991 Adhesion and detachment of the toe pads of tree frogs. *J. Exp. Biol.* **155**, 103–125.

Hui, C.-Y., Glassmaker, N. J., Tang, T. & Jagota, A. 2004 Design of biomimetic fibrillar interfaces: 2. Mechanics of enhanced adhesion. *J. R. Soc. Interface* **1**, 35–48. (doi:10.1098/rsif.2004.0005)

Martin, A., Rossier, O., Buguin, A., Auroy, P. & Brochard-Wyart, F. 2000 Spinodal dewetting of thin liquid films at soft interfaces. *Eur. Phys. J. E* **3**, 337–341. (doi:10.1007/s101890070004)

Mizuhira, V. 2004 The digital pads of rhacophorid tree-frogs. *J. Electron Microsc.* **53**, 63–78. (doi:10.1093/jmicro/53.1.63)

Nachtigall, W. 1974 *Biological mechanisms of attachment*. New York: Springer.

Peressadko, A. & Gorb, S. N. 2004 When less is more: experimental evidence for tenacity enhancement by division of contact area. *J. Adhes.* **80**, 247–261. (doi:10.1080/00218460490430199)

Persson, B. N. 1998 *Sliding friction: physical principles and applications*. New York: Springer.

Ploem, J. S. 1975 Reflection-contrast microscopy as a tool for investigation of the attachment of living cells to a glass surface. In *Mononuclear phagocytes in immunity, infection and pathology* (ed. R. van Furth), pp. 405–421. Oxford: Blackwell Scientific Publications.

Radhakrishnan, V. 1998 Locomotion: dealing with friction. *Proc. Natl Acad. Sci.* **95**, 5448–5455. (doi:10.1073/pnas.95.10.5448)

Rädler, J. & Sackmann, E. 1993 Imaging optical thicknesses and separation distances of phospholipid vesicles at solid surfaces. *J. Phys. II* **3**, 727–748. (doi:10.1051/jp2:1993163)

Reynolds, O. 1886 On the theory of lubrication and its application to Mr Beauchamp Tower's experiments, including an experimental determination of the viscosity of olive oil. *Phil. Trans. R. Soc.* **177**, 157–234.

Roberts, A. D. 1971 Squeeze films between rubber and glass. *J. Phys. D Appl. Phys.* **4**, 423–432. (doi:10.1088/0022-3727/4/3/311)

Scherge, M. & Gorb, S. N. 2001 *Biological micro- and nanotribology: nature's solutions*. Berlin: Springer.

Schmidt, T., Schütz, G. J., Baumgartner, W., Gruber, H. J. & Schindler, H. 1995 Characterization of photophysics and mobility of single molecules in a fluid lipid membrane. *J. Phys. Chem.* **99**, 17 662–17 668. (doi:10.1021/j100049a030)

Sitti, M. & Fearing, R. S. 2003 Synthetic gecko foot-hair micro/nano-structures as dry adhesives. *J. Adhes. Sci. Technol.* **17**, 1055–1073. (doi:10.1163/156856103322113788)

Welsch, U., Storch, V. & Fuchs, W. 1974 The fine structure of the digital pads of Rhacophorid tree frogs. *Cell Tissue Res.* **148**, 407–416. (doi:10.1007/BF00224267)

West, G. D. 1911 On the resistance to the motion of a thread of mercury in a glass tube. *Proc. R. Soc. A* **86**, 20–25.

Wiegand, G., Neumaier, K. R. & Sackmann, E. 1998 Microinterferometry: three-dimensional reconstruction of surface microtopography for thin-film and wetting studies by reflection interference contrast microscopy (RICM). *Appl. Opt.* **37**, 6892–6905.

Zhang, X., Zhu, Y. & Granick, S. 2002 Hydrophobicity at a Janus interface. *Science* **295**, 663. (doi:10.1126/science.1066141)